applied sciences

MDPI

Article

Characterization of the Interaction of a Novel Anticancer Molecule with PMMA, PCL, and PLGA Polymers via Computational Chemistry

Edwar D. Montenegro [1], Jamylle M. Nunes [2], Igor F. S. Ramos [2], Renata G. Almeida [3], Eufrânio N. da Silva Júnior [3], Márcia S. Rizzo [4], Edson C. da Silva-Filho [5], Alessandra B. Ribeiro [6,*], Heurison S. Silva [7] and Marcília P. Costa [1,2,*]

1 Graduate Program in Material Science and Engineering, Federal University of Piauí, Teresina 64049-550, PI, Brazil; e.montenegro@ufpi.edu.br
2 Graduate Program in Pharmaceutical Sciences, Federal University of Piauí, Teresina 64049-550, PI, Brazil; jamylleemelo@gmail.com (J.M.N.); igorfrederico10@gmail.com (I.F.S.R.)
3 Department of Chemistry, Federal University of Minas Gerais, Belo Horizonte 31270-901, MG, Brazil; renag.almeida@gmail.com (R.G.A.); eufranio@ufmg.br (E.N.d.S.J.)
4 Department of Morphology, Federal University of Piauí, Teresina 64049-550, PI, Brazil; marciarizzo@ufpi.edu.br
5 Department of Chemistry, Federal University of Piauí, Teresina 64049-550, PI, Brazil; edsonfilho@ufpi.edu.br
6 CBQF—Centro de Biotecnologia e Química Fina—Laboratório Associado, Escola Superior de Biotecnologia, Universidade Católica Portuguesa, Rua Diogo Botelho 1327, 4169-005 Porto, Portugal
7 Department of Physics, Federal University of Piauí, Teresina 64049-550, PI, Brazil; heurison@ufpi.edu.br
* Correspondence: abribeiro@ucp.pt (A.B.R.); marciliapc@ufpi.edu.br (M.P.C.)

Abstract: The development of anticancer drugs is costly and time intensive. Computational approaches optimize the process by studying molecules such as naphthoquinones. This research explores the quantitative structure–activity relationship (QSPR) and molecular interactions among 2,2-dimethyl-3-((3-nitrophenyl)amino)-2,3-dihydronaphtho[1,2-*b*]furan-4,5-dione ($QPhNO_2$), a Nor-β-Lapachone derivative with anticancer properties, and the following polymers for nanoencapsulation: polymethyl methacrylate (PMMA), polycaprolactone (PCL), and poly-lactic-co-glycolic acid (PLGA). Spartan 14 optimized the compounds using density functional theory (DFT), while ArgusLab performed docking, and Discovery Studio analyzed post-docking results. Simulations indicated that polymers with larger energy gaps are more stable and less prone to deformation than $QPhNO_2$, facilitating interaction with polymer chains. The binding energies for PMMA/$QPhNO_2$, PCL/$QPhNO_2$, and PLGA/$QPhNO_2$ interactions were −4.607, −4.437, and −1.814 kcal/mol, respectively. Docking analysis revealed non-bonded interactions between polymers and $QPhNO_2$. These findings highlight the role of computational methods in nanoencapsulation and molecular characterization, guiding the development of future analogs and combinations.

Keywords: nanoencapsulation; drug–polymer interactions; molecular docking

Academic Editors: Rui Carrilho and Fábio Rodrigues

Received: 11 December 2024
Revised: 29 December 2024
Accepted: 4 January 2025
Published: 6 January 2025

Citation: Montenegro, E.D.; Nunes, J.M.; Ramos, I.F.S.; Almeida, R.G.; da Silva Júnior, E.N.; Rizzo, M.S.; da Silva-Filho, E.C.; Ribeiro, A.B.; Silva, H.S.; Costa, M.P. Characterization of the Interaction of a Novel Anticancer Molecule with PMMA, PCL, and PLGA Polymers via Computational Chemistry. *Appl. Sci.* **2025**, *15*, 468. https://doi.org/10.3390/app15010468

1. Introduction

In recent years, the process of discovering, designing, and optimizing drugs for more effective therapies has evolved rapidly. However, the costs associated with synthesizing and characterizing new compounds render drug development an expensive and labor-intensive endeavor, with many compounds failing to achieve commercial viability as drugs [1]. Consequently, a significant portion of the cost of developing new drugs is attributable to the synthesis and testing of substances that ultimately fail.

Computer-aided methods such as quantitative structure–property relationship (QSPR) modeling, analysis, and molecular interaction investigations, including molecular docking, are increasingly being employed in the early stages of drug design, optimization, and synthesis to identify descriptors more closely associated with the target property. These innovative approaches to drug development rely heavily on the mathematical modeling of physicochemical features for chemical parameter prediction and computational structure analysis [2,3]. In this sense, computational methods have proven to be powerful tools in the discovery of medicines and treatments, including those for cancer.

Cancer is a chronic disease characterized by extensive phenotypic and genotypic diversity [4]. It is currently the second leading cause of death worldwide and is projected to surpass all other causes by 2060 [4,5]. Natural products constitute a promising source for the development of antineoplastic drugs. A significant proportion of contemporary cancer therapies are derived from or inspired by the structure of natural products [6]. One such example is naphthoquinones, a class of naturally occurring compounds that exhibit structural diversity and significant potential for biological activity, including anticancer properties, as demonstrated by Nor-β-lapachone (NβL) [7–9]. The effectiveness of these compounds typically relies on their structural framework, particularly their redox systems, which include carbonyl groups that act as vital redox centers capable of generating reactive oxygen species (ROS).

ROS production is intrinsically linked to the antitumor properties of quinone compounds. The reduction process that generates high levels of ROS can be biologically catalyzed by one- or two-electron reducing enzymes, such as NADPH-cytochrome P450 reductase and NAD(P)H quinone oxidoreductase 1 (NQO1), which function as redox agents [10]. ROS formation is associated with oxidative stress and alkylation, which involves the addition of alkyl groups to cellular nucleophilic molecules. These molecules include deoxyribonucleic acid (DNA), lipids, and proteins, among other biological macromolecules. Consequently, ROS leads to cytotoxicity and cell damage [11,12].

Research has demonstrated that structural modifications of NβL, such as those in 2,2-dimethyl-3-((3-nitro-phenyl)amino)-2,3-dihydronaphtho[1,2-*b*]furan-4,5-dione (named here $QPhNO_2$), shown in Figure 1, have displayed promising anticancer activity in in vitro models. $QPhNO_2$ can adopt different conformations, particularly due to the rotational freedom of the aromatic ring containing the nitro group in the -C-NH-C- linkage (see Figure S1 in Supporting Information), allowing for better adaptation to other molecules. However, its clinical application is limited due to its high lipid solubility, hydrophobicity, and non-specific dispersion, prompting researchers to explore alternative drug delivery methods [13].

Nanoencapsulation has been proposed as a promising strategy for administering anticancer drugs. The use of nanoparticles has been shown to enhance the therapeutic efficacy of anticancer drugs, facilitate controlled and sustained release, and reduce toxic side effects [13]. This system involves encapsulating specific components in suitable materials to protect them from adverse environmental factors. Various industries benefit from this method, including medicine, cosmetics, agriculture, thermal energy storage, polymers, textiles, and self-healing materials [14–18]. The most commonly used polymers for nanoencapsulation include polymethyl methacrylate (PMMA), poly-caprolactone (PCL), and poly-lactic-co-glycolic acid (PLGA), the structures of which are illustrated in Figure 1 [19–21].

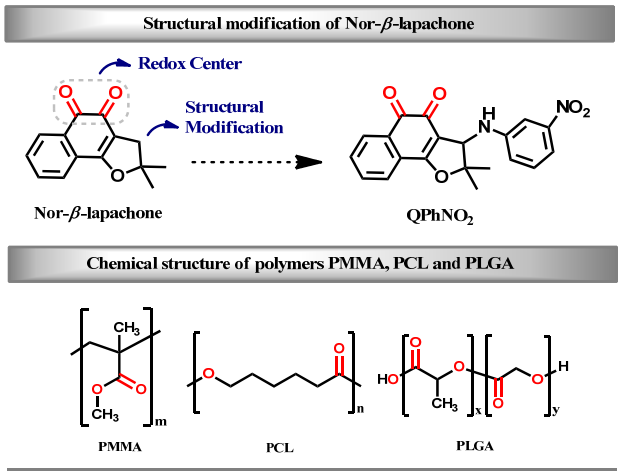

Figure 1. Illustration of the structural modification of Nor-β-lapachone for obtaining $QPhNO_2$ and polymers studied in this work: PMMA, PCL, and PLGA.

PMMA, PCL, and PLGA polymers were chosen for this study because they are biocompatible, non-toxic, and widely used in drug delivery applications [22–24]. PMMA is a thermoplastic polyester with high chemical hydrolysis resistance and high drug permeability [25,26]. It is a well-established polymer for medical applications, including drug delivery systems, lenses, dental prosthetics, and tissue engineering scaffolds [27,28]. PCL is an attractive polyester for drug delivery systems because of its slow degradation, high permeability to many drugs, and ease of functionalization [24]. PLGA is a versatile polyester, as various combinations of lactic and glycolic acid provide molecules with different properties that affect nanoparticle size, encapsulation efficiency, and release ability [29]. PMMA, PCL, and PLGA polymers are approved by the U.S. Food and Drug Administration (FDA) for biomedical applications and have been extensively studied in the development of carrier systems for anticancer drugs [22–24,30].

This theoretical study aims to characterize the QSPR molecular properties of $QPhNO_2$, PMMA, PCL, and PLGA molecules and focuses on the molecular docking simulations to identify and visualize the most likely interactions between $QPhNO_2$ and these polymers in order to identify factors influencing suitable drug release. To achieve this, we will first describe the QSPR properties, vibrational spectra, and thermodynamic characteristics derived from the geometry optimization in the density functional theory (DFT) framework, as well as the physical and quantum–chemical properties of the $QPhNO_2$ anticancer molecule and the PMMA, PCL, and PLGA polymers. This information will help determine the appropriate nanoparticle type, structure, and release profile. Finally, we will discuss the interaction outcomes using molecular docking analysis for the drug–polymer pair.

2. Materials and Methods

2.1. Computational Methods

Property calculations were conducted using Spartan'14 (Wavefunction, Inc. software, Irvine, CA, USA) software on a PC equipped with an Intel(R) Core i7 processor (4.7 GHz CPU). First, the models of the compounds studied were generated. Next, a systematic search for the best configuration was performed to establish the most stable conformations of the four compounds, presenting the minimum energy states, as depicted in Figure 2. Following the geometry optimizations, the vibrational modes, HOMO-LUMO energies, and electrostatic molecular potential were calculated using the DFT method, with the B3LYP model and the 6-311++G basis set in a vacuum for equilibrium geometry in the fundamental state [3,31–33]. A systematic study of the simulations was carried out for

polymer models with a single repeating unit with 3 or 6 in order to evaluate potential variations in the properties of interest, allowing, if applicable, extrapolation to a very large number of repeating units.

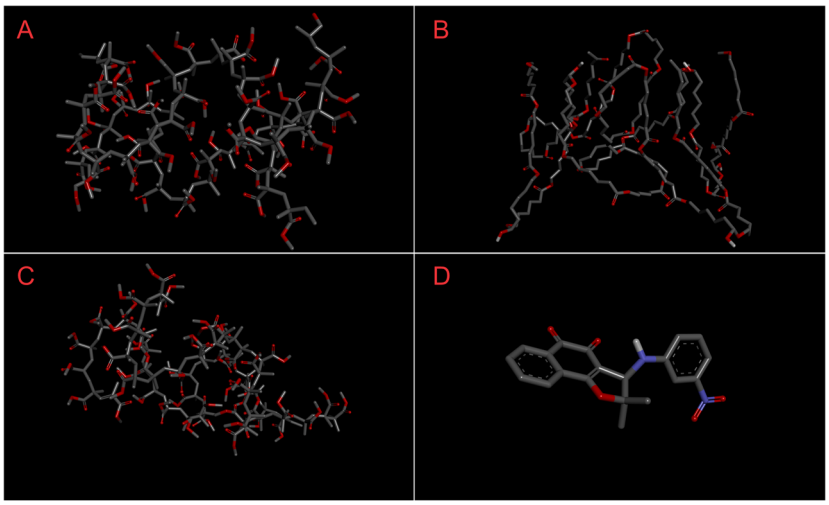

Figure 2. Optimized structures of (**A**) PMMA, (**B**) PCL, and (**C**) PLGA polymers and (**D**) $QPhNO_2$ anticancer molecule used in this work.

The vibrational modes were analyzed by comparing the infrared spectra obtained experimentally with those obtained from the in silico studies. The calculated vibrational frequencies were scaled at 0.9682. In addition, the thermodynamic characteristics of the polymers and the $QPhNO_2$ drug at various temperatures were calculated using the same method, and the correlations among enthalpy, entropy, and heat capacity with temperature were obtained from the simulations.

The study of molecular interactions was conducted using ArgusLab 4.0.1 (Richland, WA, USA), a software extensively validated for binding energy calculations and simulations of drug–polymer interactions [34,35]. The docking algorithm employed was ArgusDock, utilizing a flexible ligand and rigid polymer approach, with the AScore function applied as the default scoring method for binding energy calculations. The Universal Force Field (UFF) was used for ligand structure optimization before docking. The docking grid was configured to cover the entire polymer interaction site with a resolution of 0.4 Å, and the accuracy setting was kept in regular mode for a balanced trade-off between precision and computational efficiency [35–37]. For visualization and characterization of interactions, Discovery Studio Visualizer software v21.1.0.20298 (BIOVIA, San Diego, CA, USA) was used.

The quantum properties of the molecules were determined from the values obtained for the HOMO and LUMO energies, as follows: the energy gap (HOMO-LUMO) ($\Delta E = E_{LUMO} - E_{HOMO}$), the ionization potential ($I = -E_{HOMO}$), the electronic affinity ($A = -E_{LUMO}$), the electronegativity ($\chi = (I + A)/2$), the global hardness ($\eta = (I - A)/2$), global sweetness ($\sigma = 1/\eta$), chemical potential ($\mu = (E_{LUMO} + E_{HOMO})/2$), the global electrophilicity index ($\omega = \mu^2/2\eta$). All these parameters are important descriptors in intermolecular interactions and significantly affect the interaction between the polymers and the drug to be encapsulated [38,39].

2.2. Material and Instrumentation

For the experimental FTIR measurements, PCL, PLGA, and PMMA polymers were purchased from Sigma-Aldrich Chemical Corporation (St. Louis, MO, USA). All materials were used as received. The $QPhNO_2$ compound was synthesized at the chemical synthesis

laboratory at the Federal University of Minas Gerais, Brazil. Infrared spectra were acquired using a Perkin Elmer Spectrum One Fourier transform infrared (FTIR) spectrometer (Perkin Elmer, Shelton, CO, USA).

3. Results and Discussion

The HOMO (the outermost orbital containing electrons) is related to the ability to donate electrons, while the LUMO (the lowest unoccupied molecular orbital) represents the ability to accept electrons. These frontier molecular orbitals are crucial in illustrating the electronic properties of a substance and have significant roles in identifying active sites, determining kinetic stability, and influencing the chemical reactivity of molecules. These electronic orbitals are fundamental to the reactivity of chemical compounds. The formation of transition states in reactions occurs through the interaction of the HOMO and LUMO border orbitals of reacting species [38].

Quantitative structure–property relationship (QSPR) data describe the structural and physicochemical information. Energy values of these orbitals, along with other molecular properties derived from simulations, are presented in Figure 3. for $QPhNO_2$ and structures with six repeating units, which are representative of the polymer. This approach assumes that the interaction of $QPhNO_2$ effectively occurs only with those segments closest to it, making the length of the polymer chain less significant if the polymer chain has a few or hundreds of repeating units. Since the $QPhNO_2$ molecule has a chiral center (see Figure S1), which allows the formation of two enantiomorphic forms, it was not possible to observe significant differences between the values obtained from our simulations (data shown in Supporting Information). This result is important because, in our simulations, $QPhNO_2$ is flexible, adopting any configuration that allows anchoring and minimizes interaction energy.

The lipophilicity of substances is linked to the octanol–water partition coefficient (logP), which evaluates the ability of compounds, such as $QPhNO_2$ and PCL, PLGA, or PMMA polymers, to traverse the intestinal epithelium (logP > 0 indicates lipophilic substances, but logP < 0 indicates hydrophilic substances). The method of Ghose, Pritchett, and Crippen [40] is used to determine log P values [41]. Lipinski's Rule of Five [42] stipulates that the logP for drug molecules should be less than 5, based on the observation that the majority of orally absorbed compounds exhibit logP < 5. LogP and PSA can be correlated when assessing potential drugs using the criteria stated by Hughes et al. [43], which include log P < 4 and PSA > 75 Å2, as can be seen for $QPhNO_2$ [44].

Polarizability provides information about electrostatic interactions that arise when an ion or dipole induces a temporary dipole in an adjacent molecule. Those values can be observed in Table 1. While polarizability is defined by the electronic distribution throughout the molecule, the dipole moment depends on the spatial configuration of the molecule. These results emphasize the importance of understanding molecular properties and their implications in drug development and optimization.

3.1. Frontier Molecular Orbitals

Based on the optimized geometry of the PMMA, PCL, PLGA, and $QPhNO_2$ molecules, we present the results of frontier molecular orbitals obtained from modeled molecules shown in Figure 1. Molecular frontier orbitals are crucial indicators of a molecule's reactivity, represented by the difference between the gap $\Delta E = E_{LUMO} - E_{HOMO}$ values. Therefore, molecules that are chemically stable are indicated by the larger value of gap ΔE. To observe how the frontier orbitals behave in each repeating unit, the surfaces presented in Figure 3 correspond to the highest occupied molecular orbital (HOMO) and the lowest unoccupied molecular orbital (LUMO) for a group of six repeating units. Our simulations of the

polymers with one, three, or six repeating unities showed that several properties changed, but not all. For example, band gap values vary little with increasing molecular weight. (For more details, see Table S1 in Supporting Information).

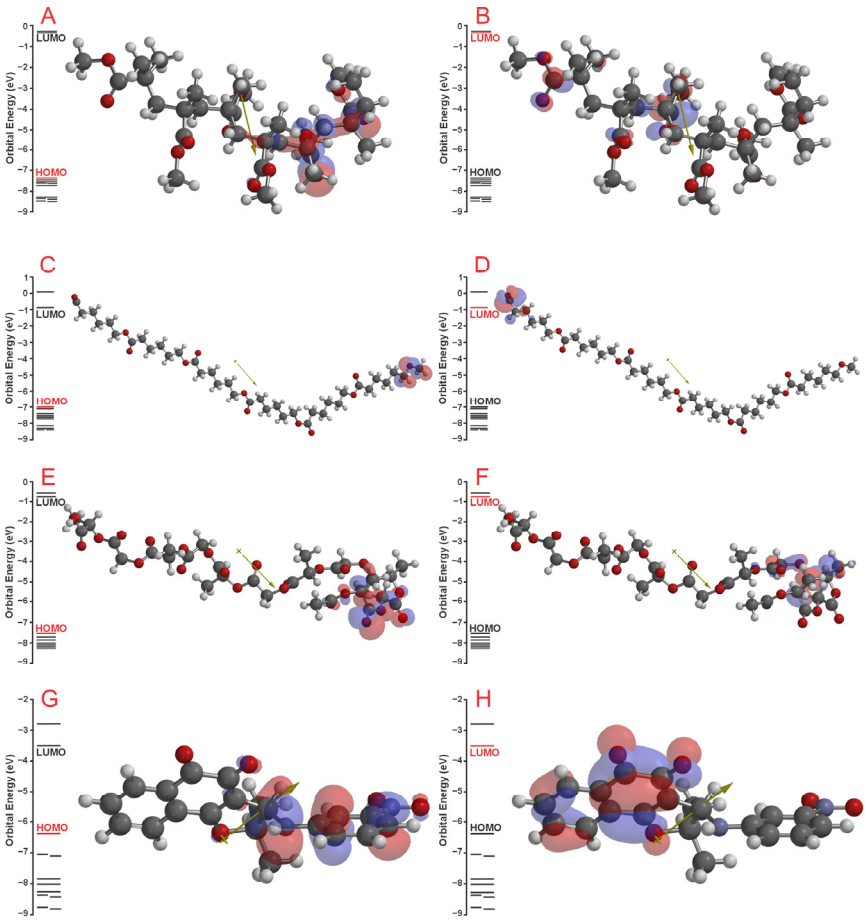

Figure 3. HOMO-LUMO energy diagrams (ground state) for different polymers and compounds, each represented with six repeating units. In each image pair, the letters indicate the corresponding orbital: (**A**,**B**) represent PMMA with HOMO and LUMO, respectively; (**C**,**D**) illustrate PCL; (**E**,**F**) show PLGA; and finally, (**G**,**H**) display $QPhNO_2$, highlighting the variation in electronic distribution between HOMO and LUMO in each material. The arrows represent the dipole moment vector of the molecule, indicating the direction and magnitude of the molecular polarity. The arrow points from the region of partial positive charge to the region of partial negative charge, and its length reflects the magnitude of the dipole moment.

The interaction between molecules occurs through the strong interaction between the HOMO region of one molecule and the LUMO region of another. It is expected that a molecule with a smaller orbital gap value is more polarizable and exhibits a significant degree of intramolecular charge transfer from the electron donor to the electron acceptor conjugation, which can influence the biological activity of the molecule [2,6,38]. The values of these selected properties can be seen in Table 2.

Considering the information in Table 2 and the frontier molecular orbital (FMO) analysis (Figure 3), it is possible to infer important information about the potential interactions between the polymers and the $QPhNO_2$ molecule. As noted above, PMMA, PCL, and PLGA have high energy gaps, specifically 7.01 eV, 6.11 eV, and 6.78 eV, respectively, indicating more stable molecules compared to $QPhNO_2$ (2.78 eV). These properties may contribute to the stability of the encapsulated $QPhNO_2$ molecule, protecting it from undesired interactions with other molecules in the biological environment and preventing premature degradation.

Table 1. Calculated molecular properties for $QPhNO_2$, PMMA, PCL, and PLGA molecules, utilizing the DFT approach, B3LYP model, and 6-311++G basis set in a vacuum for equilibrium geometry in the ground state.

	$QPhNO_2$	PMMA	PCL	PLGA
Structural formula	$C_{20}H_{16}N_2O_5$	$(C_5H_8O_2)_6$	$(C_6H_{10}O_2)_6$	$(C_3H_4O_2)_6$ + $(C_2H_2O_2)_6$
Weight (amu)	364.357	630.722	700.907	782.610
Dipole moment (Debye)	9.05	6.54	2.97	14.01
HOMO energy (eV)	−6.29	−7.37	−7.02	−7.53
LUMO energy (eV)	−3.51	−0.36	−0.91	−0.75
PSA (Å^2)	84.461	115.159	124.564	254.494
log P	3.49	7.14	5.18	3.49
HBD count	1	0	0	0
HBA count	7	0	7	0
Polarizability (10^{-30} m^3)	68.99	93.52	102.04	96.75

Table 2. Calculated quantum chemical parameters of the compounds studied in this work.

Quantum Parameters	$QPhNO_2$	PMMA	PCL	PLGA
Gap energy (ΔE) (eV)	2.78	7.01	6.11	6.78
Ionization energy (I) (eV)	6.29	7.37	7.02	7.53
Electron affinity (A) (eV)	3.51	0.36	0.91	0.75
Electronegativity (x) (eV)	4.90	3.87	3.97	4.14
Hardness (η) (eV)	1.39	3.51	3.06	3.39
Softness (σ) (eV^{-1})	0.72	0.29	0.33	0.29
Chemical potential (μ) (eV)	−4.90	−3.87	−3.97	−4.14
Global electrophilicity (GE) (eV)	8.64	2.13	2.57	2.53

The calculated energy gaps (ΔE) for the three polymers obtained using DFT calculations (B3LYP/6-311++G) align well with the reported ranges in the literature. For instance, theoretical and experimental values for PMMA typically fall within the range of 6.8–7.2 eV [45,46], while similar consistency is observed for PCL [38] and PLGA [47]. These results reinforce the reliability of our computational approach, demonstrating its ability to predict quantum chemical parameters.

By examining the frontier molecular orbitals (HOMO and LUMO) of the polymers, we observe that the reactive regions are located near the end of the backbone. This is particularly evident for PCL, indicating that the number of intermediate repeating units is not significantly important for the location or energy values of these orbitals in this case. For the $QPhNO_2$ molecule (Figure 3), it is possible to identify preferred interaction sites and gain a better understanding of how encapsulation occurs. This information can be useful for optimizing the encapsulation efficiency.

It is important to emphasize that different polymers may exhibit distinct encapsulation properties due to their chemical structures and physical properties. For example, PCL and PLGA are biodegradable and biocompatible polymers, making them ideal in biomedical applications, including drug nanoencapsulation [20,21]. These polymers may be particularly suitable for controlled-release systems of molecules like $QPhNO_2$ due to their ability to degrade in the body and release the encapsulated drug in a controlled manner. In contrast, PMMA is a non-biodegradable polymer, which may limit its applicability in some biomedical applications [19]. However, its optical and insulating properties can be exploited in other applications, such as protecting the $QPhNO_2$ molecule from light or undesired redox reactions [48].

According to Table 2, $QPhNO_2$ has a higher electronegativity value (4.90 eV) compared to the polymer molecules. Electronegativity is defined as a measure of a molecule's ability to attract electrons to itself in a bond. As shown, the electronegativity values follow the trend PMMA < PCL < PLGA (3.87 < 3.97 < 4.14). For the most stable conformers of $QPhNO_2$, PMMA, PCL, and PLGA compounds, additional quantum chemical parameters, such as ionization potential (I), electron affinity (A), chemical potential (μ), global electrophilicity index (GE), and hardness (η), are also calculated and reported in Table 2.

The chemical potential (μ) represents the tendency of electrons to escape from a stable system. The negative chemical potential indicates that a complex is stable and does not spontaneously decompose into its elements. Hardness refers to the resistance to the deformation of the electronic cloud of the chemical system under minor disturbances encountered during the chemical process. From the values shown in Table 2, we can observe that hardness increases in the following order: $QPhNO_2$ < PCL < PLGA < PMMA (1.39 < 3.06 < 3.39 < 3.51). A soft, more reactive molecule is one with a small HOMO-LUMO gap as opposed to one with a big HOMO-LUMO gap. The global electrophilicity index (ω) assesses the decrease in energy due to the maximum flow of electrons between the donor and acceptor calculated from the HOMO-LUMO energy values.

3.2. Electrostatic Potential Mapping (EPM)

Another parameter for examining a molecule's chemical reactivity is electrostatic potential mapping (EPM). In hydrogen bond interactions, it is a crucial tool for locating reactive regions for nucleophilic or electrolytic attacks. It is also important for understanding the biological recognition process 2. Compared to the energy gap between the HOMO and LUMO orbitals, which only considers the size of the gap, EPM clearly shows the regions of the molecule most prone to positive or negative potentials. Figure 4 shows the electrostatic potential maps for the four molecules, highlighting the hydrophilic (negative and positive potential) and hydrophobic (neutral) regions.

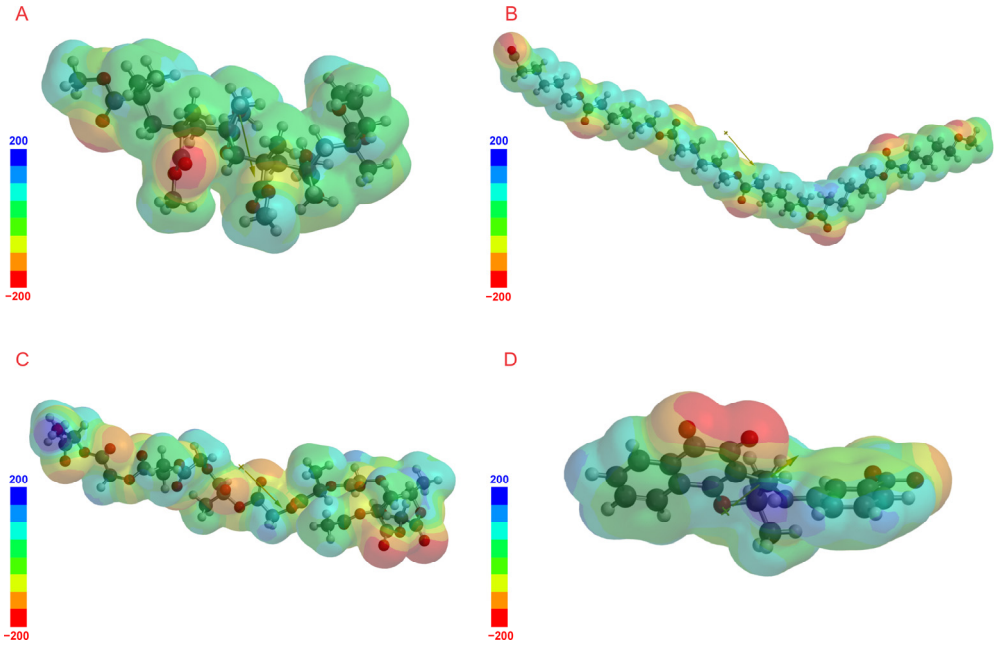

Figure 4. Electrostatic potential map (EPM) of (**A**) PMMA, (**B**) PCL, (**C**) PLGA with 6 repeating units, and (**D**) $QPhNO_2$, displayed in ball-and-stick representation.

In all polymers studied here, the negative potentials are located on the double-bonded oxygen atom (negative potential sites are found on electronegative atoms, while positive

potential sites are around the hydrogen atoms). These graphs provide information about the regions from which the compound may engage in non-covalent interactions [49], presenting the lowest value of −155.40 kJ/mol and the highest value of 128.30 kJ/mol for PMMA. A similar behavior was observed in the PCL molecule, with a minimum negative value of −175.40 kJ/mol and a positive electrostatic potential reaching a maximum value of 127.50 kJ/mol. PLGA has the lowest electrostatic potential value near the carbon atom, with a double bond of −192.30 kJ/mol and the highest positive value of 116.90 kJ/mol. Finally, the most negative value of −177.20 kJ/mol and the most positive value of 198.40 kJ/mol were found for the $QPhNO_2$ compound.

Thus, we can conclude that the three polymer molecules used in this study exhibit hydrophilic regions (positive and negative electrostatic potential) and hydrophobic regions (regions with neutral electrostatic potential), as does the $QPhNO_2$ molecule. The negative EPM regions, in red, correspond to electrophilic reactivity, while the positive region, shown in blue, corresponds to nucleophilic reactivity. This is because the electrostatic force plays an important role in the interaction between $QPhNO_2$ and the polymers.

3.3. Local Ionization Potential Map (LIPM)

When assessing chemical reactivity and selectivity in terms of electrophilic reactions, the ionization potential—which reflects the overlap of the ionization energy on the electronic density—is a valuable metric [50]. In Figure 5, colors toward red represent negative values, while colors toward blue represent positive values. Electrostatic potentials on molecular surfaces can be complemented by local ionization potential maps when processes involve charge transfer and bond formation, as in the electrophilic attacks [51].

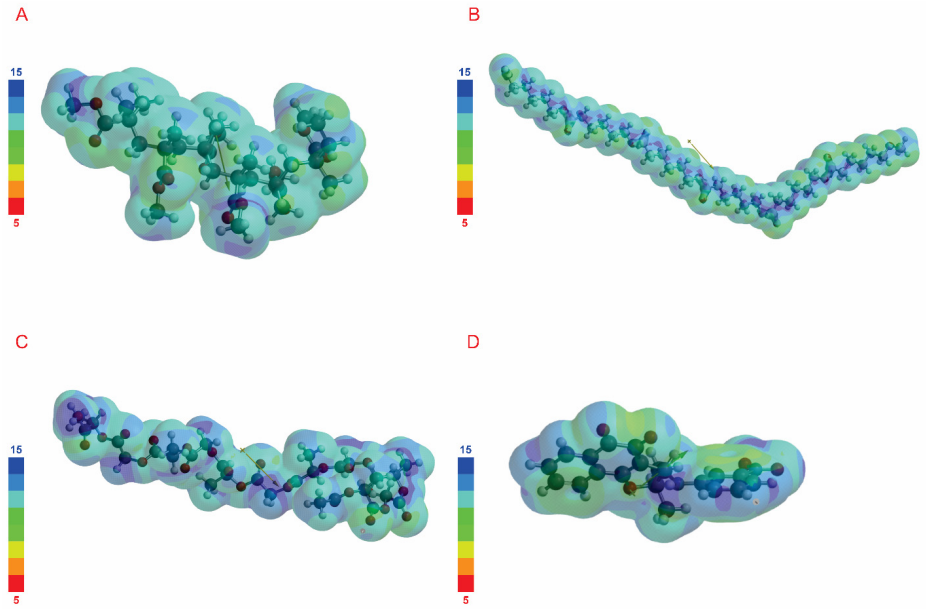

Figure 5. Map of the local ionization potential (LIPM) of (**A**) PMMA, (**B**) PCL, (**C**) PLGA with six repeating units, and (**D**) $QPhNO_2$.

The analysis of the local ionization potential map (LIPM) (Figure 5) provides significant insights into the electronic distribution and reactivity of the studied molecules. The three polymer molecules exhibit both hydrophilic regions (positive and negative electrostatic potential) and hydrophobic regions (neutral electrostatic potential). Similarly, the $QPhNO_2$ molecule also displays positive and negative electrostatic potential values, indicating the presence of hydrophilic and hydrophobic regions. The LIPM reveals specific areas with varying ionization potentials. The $QPhNO_2$ molecule demonstrates the most negative and

positive ionization potentials, respectively, with values of 9.41 eV and 14.15 eV. These values indicate regions with varying tendencies for electrophilic and nucleophilic interactions, respectively. The negative EPM regions, indicated in red, correspond to electrophilic reactivity, whereas the positive regions, shown in blue, are responsible for nucleophilic reactivity. These findings are significant for elucidating the chemical behavior and potential applications of these molecules in drug delivery and polymer science.

3.4. Vibrational and Thermodynamic Characterization

In silico investigations were conducted to describe the theoretical characteristics of the four molecules under study, including their vibrational and thermodynamic modes. These characteristics are essential for characterizing the combined polymer/drug systems that will form the nanocapsules. Figure 6 presents the theoretical spectra obtained from the in silico studies in the region from 500 to 4000 cm^{-1}. The spectra obtained experimentally are presented in Figure 7. By comparing the two sets of spectra, it can be observed that they are very similar, highlighting some vibrational peaks, as explained in Table 3.

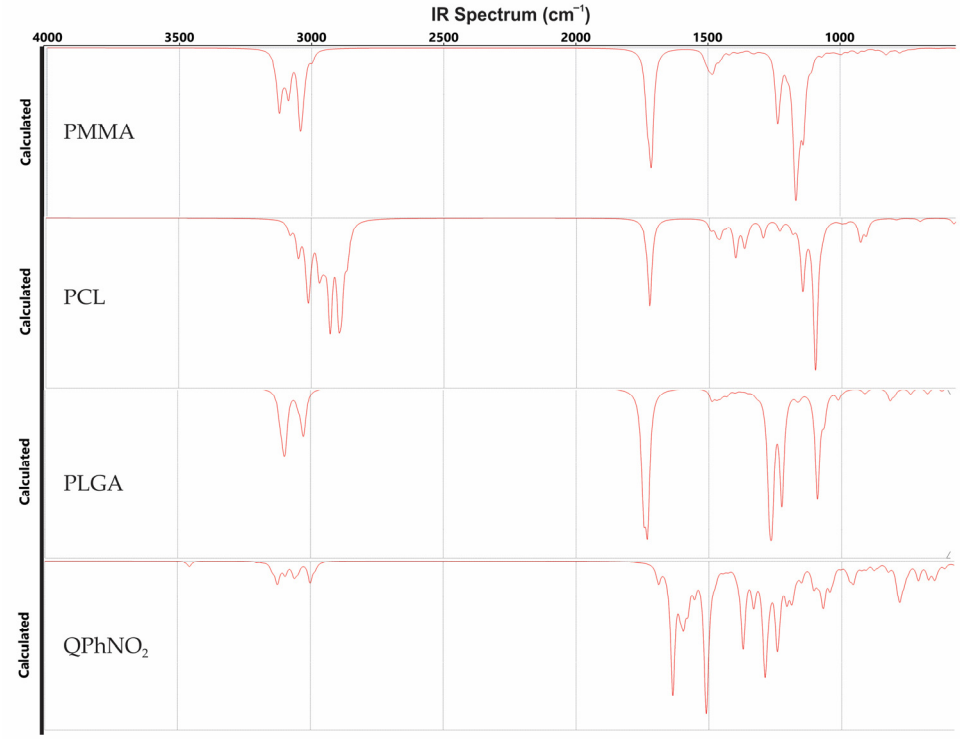

Figure 6. Theoretical FTIR spectra of PMMA, PCL, PLGA, and $QPhNO_2$, respectively, obtained by computer simulation.

In both the theoretical and experimental IR spectra, it is evident that PMMA, PCL, and PLGA display characteristic peaks of C=O stretching vibrations at 1726 cm^{-1}. The calculated C=O stretching vibrations in the region of 1797 cm^{-1} show a shift of 71 cm^{-1}, which is in good agreement with experimental assignments in the regions of 1720 to 1740 cm^{-1}, as referenced by CH_2 bending modes at 1361, 1397, and 1473 cm^{-1} and CH_2 asymmetric stretching at 2942 and symmetric stretching at 2862 cm^{-1} are observed. The C=O=C stretching vibrations yield peaks at 1042, 1107, and 1233 cm^{-1}.

The FTIR spectra of $QPhNO_2$ clearly show the formation of urethane groups (from isocyanate segments). The symmetric and asymmetric stretching vibrations of N-H correspond to the broad absorption bands near 3329–3337 cm^{-1}, while the medium–strong peak at 1530–1535 cm^{-1} confirms the in-plane bending vibration of N-H. Strong absorption peaks at 1665–1720 cm^{-1} and 1221 cm^{-1} are typical for the stretching vibration of esters

CO and the asymmetric stretching vibration of C-O (from N-CO-O), respectively. The weak peak near 916 cm^{-1} is due to the N-CO-O symmetric stretching vibration. The 1601 cm^{-1} absorption peak is caused by the vibration of C-C in benzene. These values show good agreement with theoretical calculations.

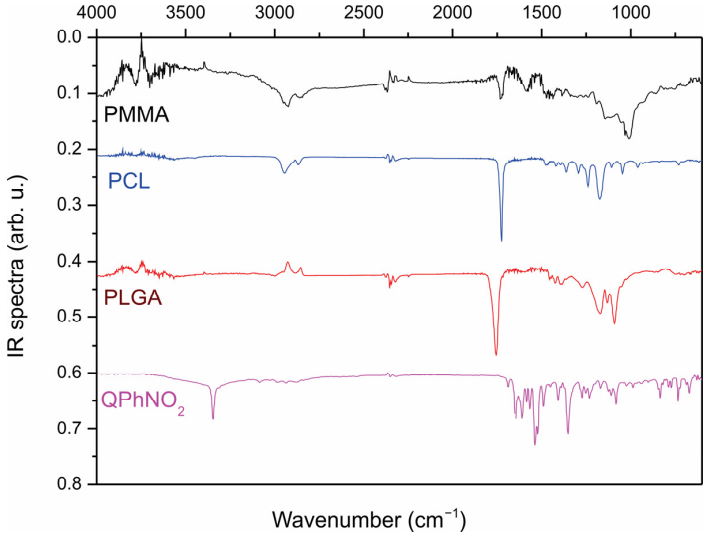

Figure 7. Experimental FTIR spectra of PMMA, PCL, PLGA (as received), and $QPhNO_2$.

Thermodynamic data were obtained and can be used to calculate additional thermodynamic properties, such as energies and reaction directions, based on correlations between thermodynamic functions. These analyses provide insights into the stability and reactivity of the polymer/drug systems, contributing to a better understanding of their behavior under different conditions. Thermodynamic parameters, such as entropy (S), enthalpy (H), and heat capacity (Cv), are essential for characterizing complex systems composed of two or more molecular components. These parameters, calculated for the PMMA, PCL, PLGA polymers, and the $QPhNO_2$ drug, were determined using the DFT/B3LYP/6-3 11++G method at 298.15 K (room temperature) and are shown in Table 4. Additionally, these parameters were computed across a temperature range from 100 K to 500 K. It should be noted from the results that these thermodynamic parameters depend on temperature, as does the way in which the vibrational intensities of molecules increase with temperature. A quadratic polynomial function was used to fit the equations relating temperatures to entropy, heat capacity, and enthalpy, as well as the corresponding adjustment factors (R^2).

Figure 8 shows the correlation graphs of these thermodynamic functions. The corresponding adjustment equations for enthalpy, heat capacity, and the entropy of PMMA, PCL, PLGA, and $QPhNO_2$ are shown in Table 5. All parameters show increasing behavior with temperature, except for enthalpy.

These data can be used to compute other thermodynamic energies based on the relationships between thermodynamic functions and to estimate the directions of chemical reactions in accordance with the second law of thermodynamics within the thermochemical field.

3.5. Drug–Polymer Interaction

The physicochemical properties of the three polymers and the $QPhNO_2$ molecule can be used to understand how $QPhNO_2$ interacts with the three polymers, PMMA, PCL, and PLGA, which can encapsulate molecules. Thus, the interactions between $QPhNO_2$ and the polymers were studied to identify the most suitable candidate for nanoencapsulation. Figure 9 displays the results obtained. In docking interactions, $QPhNO_2$ was configured as a flexible ligand in such a way that it could adopt conformations that minimize the inter-

action energy in each case. This observation is particularly reasonable when considering the hardness values presented in Table 2: $QPhNO_2$ < PCL < PLGA < PMMA. The respective binding energies found are PMMA/$QphNO_2$: −4.60691 kcal/mol, PCL/$QPhNO_2$: −4.43676 kcal/mol, and PLGA/$QPhNO_2$: −1.81392 kcal/mol, indicating weak interactions in comparison with other molecular systems (especially the PLGA/$QPhNO_2$ interactions), such as the protein interactions, with a ligand, which easily varies between −10 to around −150 kcal/mol.

Table 3. The frequencies (in cm^{-1}) of the main vibrational modes calculated by the DFT/B3LYP methods using the base set 6-311++G and experimental PMMA, PCL, PLGA, and the drug $QPhNO_2$.

Molecules	Main Peaks	Freq. Vibrations Theoretical	Freq. Vibrations Experimental
PMMA	(CH_3) Symmetrical stretch	3177	2981
	(CH_3) Symmetrical stretch	3058	2885
	(C=O) Symmetrical stretch	1797	1726
	(C, H) Scissors (angular folding)	1526	1145
	(C-O) Asymmetric Stretch	1360	-
PCL	(C-H) Asymmetric elongation	3105	2947
	Asymmetric elongation	3009	2873
	Asymmetric elongation	1824	1724
	Scissors (fold)	1337, 1275	1242, 1170
	(C-O-C) Asymmetric elongation	1206	1049
PLGA	(C-H) Symmetrical elongation	3682	3649
	(C-H) Symmetrical elongation	3158	3087
	(CH_3) Symmetrical elongation	3075	3020
	(C-H) Asymmetric elongation	3000	2999
	(O-C-O) Asymmetric elongation	1865	1753
	Balance sheet	1265	1087
	(O-H) Balance sheet	594	698
$QPhNO_2$	(N-H) Asymmetric elongation	3432	3346
	(C-C) Asymmetric elongation	1743	1649
	(C-H) Scissors (fold)	1669	1537
	(C-H) Balance sheet	1561	1352
	(C=C-C) Asymmetric elongation	1332	1083

Table 4. Thermodynamic parameters at room temperature of PMMA, PCL, PLGA, and $QPhNO_2$ molecules.

Molecule	H°	C_v	S°
PMMA	−345.65 au	88.41 J/mol	347.03 J/mol
PCL	−464.71 au	132.08 J/mol	417.24 J/mol
PLGA	−571.32 au	115.97 J/mol	393.56 J/mol
$QPhNO_2$	−1241.529 au	250.30 J/mol	548.43 J/mol

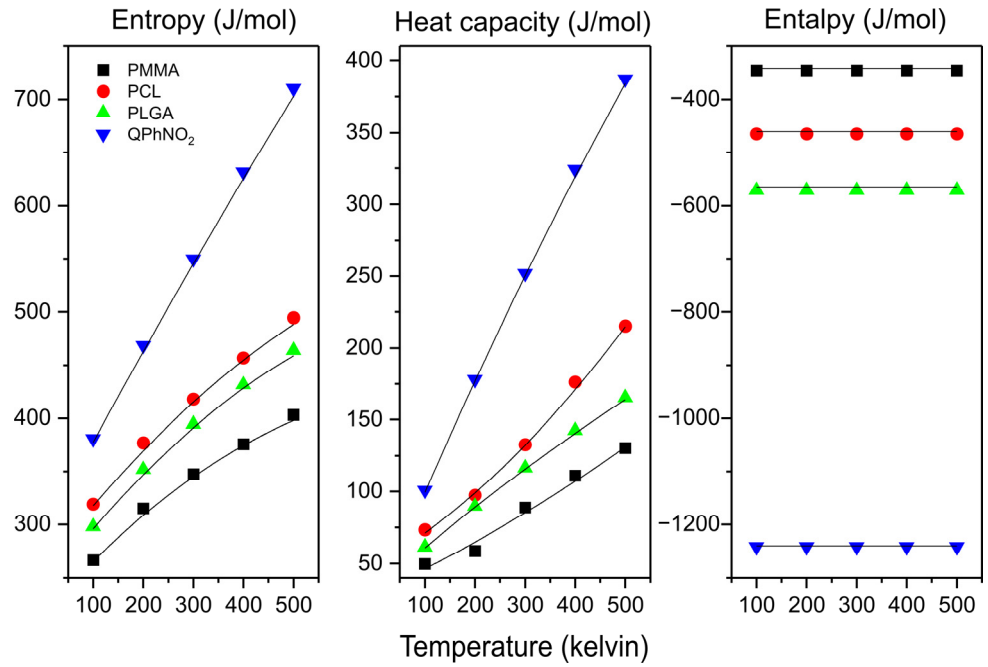

Figure 8. Thermodynamic parameters of PMMA, PCL, PLGA, and $QPhNO_2$ molecules: entropy, heat capacity, and enthalpy. The lines are the theoretical adjustments described in Table 5.

Table 5. Thermodynamic parameters H, S, and C_v obtained through theoretical adjustments using a second-order polynomial equation as a function of temperature T.

Functional Form		$a + b\,T + c\,T^2$			
		a	***b***	***c***	$\mathbf{R^2}$
Enthalpy	PMMA	−345.66	1.10×10^{-5}	5.00×10^{-8}	0.99535
	PCL	−464.72	1.71×10^{-5}	7.14×10^{-8}	0.99591
	PLGA	−571.33	2.62×10^{-5}	4.24×10^{-8}	0.96821
	$QPhNO_2$	−1241.54	2.10×10^{-5}	15.0×10^{-8}	0.99969
Entropy	PMMA	218.44	0.53	-3.29×10^{-4}	0.99673
	PCL	262.22	0.61	-3.06×10^{-4}	0.99616
	PLGA	240.35	0.62	-3.43×10^{-4}	0.99833
	$QPhNO_2$	292.66	0.90	-1.30×10^{-4}	0.99938
Heat capacity	PMMA	30.10	0.16	9.31×10^{-5}	0.99980
	PCL	48.88	0.20	2.70×10^{-5}	0.99937
	PLGA	31.14	0.31	-8.29×10^{-5}	0.99991
	$QPhNO_2$	17.76	0.85	-21.31×10^{-5}	0.99980

The binding energies calculated for PMMA/$QPhNO_2$, PCL/$QPhNO_2$, and PLGA/$QPhNO_2$ fall within typical ranges observed for non-covalent interactions in drug–polymer systems, generally reported between −1 and −6 kcal/mol [38,45–47]. Lower (more negative) binding energy values suggest stronger molecular affinity, while less negative values indicate weaker but still relevant interactions for encapsulation purposes. These findings are consistent with results from similar studies investigating molecular docking for drug delivery applications [38,47]. Non-covalent interactions, such as Van der Waals forces and hydrogen bonds, are essential for the efficacy of drug delivery systems, directly affecting encapsulation efficiency and release profiles [52,53]. These weaker interactions facilitate

controlled drug release, allowing factors like diffusion, polymer degradation, and surfactants to influence the release profile. By correlating binding energies, polymer properties, and encapsulation dynamics, we conclude that the observed interactions are sufficient to ensure encapsulation stability and effective controlled release of $QPhNO_2$ across different applications. Together, these data validate our methodology and provide confidence in the accuracy of the computational predictions presented in this work.

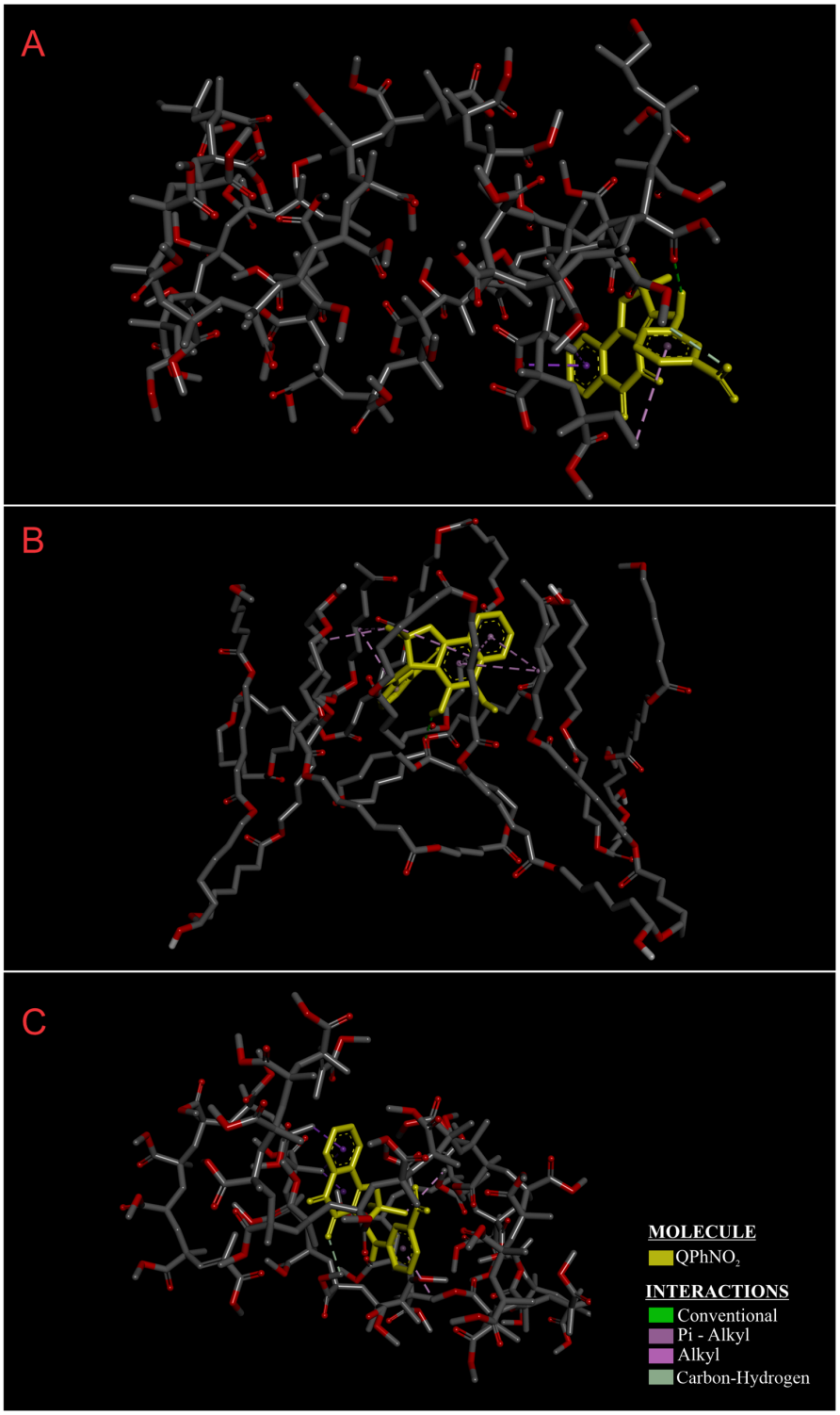

Figure 9. Simulations of the molecular interactions among (**A**) PMMA/$QPhNO_2$, (**B**) PCL/$QPhNO_2$, and (**C**) PLGA/$QPhNO_2$. $QPhNO_2$ is highlighted in yellow. The distances between interacting groups are also shown (in angstroms).

Figure 9A illustrates the interaction between PMMA and $QPhNO_2$. Using Discovery Studio, five favorable interactions were identified, involving pi–sigma, pi–alkyl interactions (hydrophobic interaction), and a non-classical hydrogen bond. One of the pi–sigma interactions occur between the PMMA carbon atom and the aromatic ring of the $QPhNO_2$ molecule. The other pi–sigma interaction involves the same carbon atom and another ring containing two double carbon bonds. Non-covalent interactions involving pi systems are critical for biological processes, such as protein–ligand recognition [1]. The other interactions are pi–alkyl between the carbon atom and the second aromatic ring, between the last carbon atom and the second aromatic ring, and between the same atom and the molecule's central region.

Figure 9B shows the interaction between PCL and $QPhNO_2$. Four favorable interactions were identified: one pi–sigma bond (hydrophobic interaction) between a carbon atom and an aromatic ring and three pi–alkyl bonds (hydrophobic interaction) between the molecule's center and carbon atoms in the aromatic rings.

Lastly, Figure 9C depicts the interaction between PLGA and $QPhNO_2$. This is the weakest interaction among all polymers studied. A conventional hydrogen bond is observed between the PLGA hydrogen atom and the double-bonded oxygen, a pi-donor-type bond between hydrogen and the aromatic ring, and a pi–alkyl bond between a carbon atom and the aromatic ring. It is known that pi interactions generally contribute to inhibitor binding because they are not affected by solvation or desolvation processes. Therefore, changes in the enthalpy/entropy ratio on free binding energy may be minimal. Additionally, we observe unfavorable bonds between the oxygen of the PLGA and the steric group of the $QPhNO_2$.

As observed, both polymers of the $QPhNO_2$ molecule exhibited high lipophilicity, which hindered the medication delivery process. Lipophilicity refers to a compound's ability to dissolve in fats, oils, lipids, and non-polar solvents. In drug discovery, LogP is widely used as a quantitative measure of lipophilicity, offering insights into parameters such as solubility, cellular permeability, plasma protein binding, and metabolic stability [54–56]. These properties are essential for understanding the interaction behavior of drug molecules with polymeric matrices, directly influencing encapsulation efficiency and drug release profiles. The purpose of encapsulation is to protect the drug molecule so that it can reach the target tissue. However, to facilitate this delivery process, a surfactant solution, such as Tween® 80 (also known as Polysorbate 80), is often added after preparing the polymer and drug solutions. The surfactant helps improve the in vitro dissolution of the drug in water, thereby accelerating the release process and simulating an in vivo administration. Therefore, taking into account how the surfactant interacts with the (polymer + $QPhNO_2$) system will help understand the drug delivery dynamics.

Figure 10 shows our best simulations of Tween® 80 with the models of Figure 9. The results show that Tween® 80 interacts preferentially with the polymeric matrix in all three cases, avoiding interacting with $QPhNO_2$. Furthermore, minimal interaction was observed between the surfactant and the polymers, as described below: (PMMA + $QPhNO_2$)/Tween® 80: −0.392426 kcal/mol, (PCL + $QPhNO_2$)/Tween® 80: −0.383648 kcal/mol, and (PLGA + $QPhNO_2$)/Tween® 80: −0.31488 kcal/mol, indicating very weak interactions, especially in comparison with the polymer/drug interaction. Thus, although there is surfactant in the nanocapsule, it does not substantially interfere with the drug delivery process.

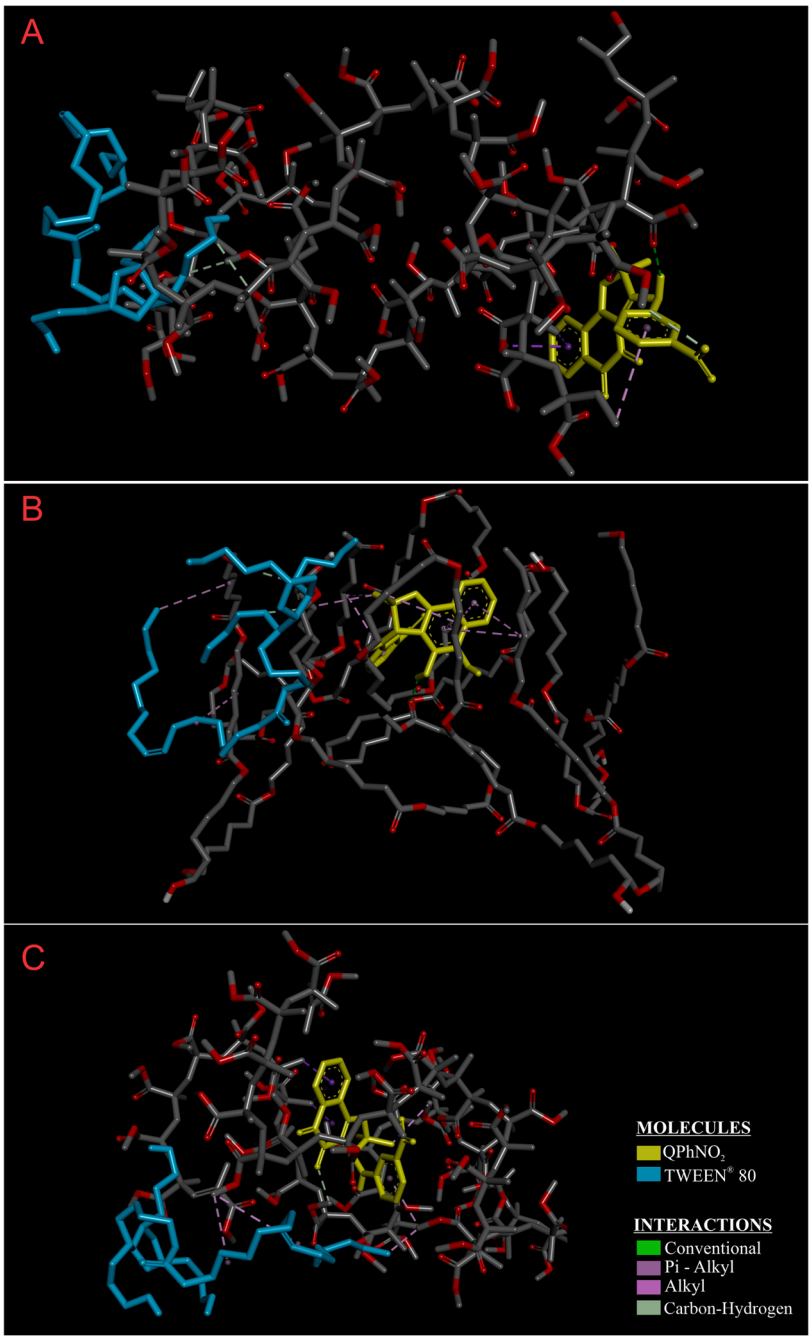

Figure 10. Simulations of molecular interactions (**A**) (PMMA + $QPhNO_2$)/Tween® 80, (**B**) (PCL/$QPhNO_2$)/Tween® 80, and (**C**) (PLGA/$QPhNO_2$)/Tween® 80. $QPhNO_2$ and Tween® 80 are highlighted in yellow. Distances between interacting groups are indicated in angstroms (Å).

These findings suggest that the molecules interact favorably for binding, with the most effective interaction occurring between $QPhNO_2$ and PCL, followed by the interaction between $QPhNO_2$ and PMMA, and the weakest between $QPhNO_2$ and PLGA. As a result, it is possible to tune the release mechanism according to the specific application of the drug, taking into account factors such as pH, temperature, ionic strength, and other environmental conditions in which it will be applied.

In this study, the polymers were maintained as rigid structures, while the molecule (ligand) was considered a flexible structure. The decision to preserve the polymer chains in a rigid state during the molecular docking simulations was made to reduce computational complexity and facilitate a clear and objective examination of the initial interactions between

$QPhNO_2$ and the selected high-molecular-weight polymers. While it is acknowledged that this simplification may underestimate subtle conformational effects, previous studies indicate that key interaction sites, such as hydrogen bonds and hydrophobic contacts, are predominantly located in accessible surface regions or polymer ends, which are less affected by large-scale structural rearrangements. Consequently, the rigid docking model persists as a computationally efficient framework that retains the fundamental aspects of drug–polymer interactions. This approach has been widely adopted due to its ability to maintain a balance between computational feasibility and predictive accuracy when analyzing drug–polymer affinity and binding behavior [37,57,58].

This investigation used molecular docking to identify binding affinities and interaction sites between QPhNO2 and the polymers. However, molecular dynamic (MD) simulations may provide a deeper understanding of the temporal stability and conformational changes of these complexes [59–61].

4. Conclusions

This study combined experimental and theoretical analyses to investigate the potential interactions among PCL, PMMA, and PLGA polymers proposed for the encapsulation of the anticancer compound $QPhNO_2$. The quantum properties of the molecules were calculated from HOMO and LUMO energies, which showed that $QPhNO_2$ exhibited the low gap value E_LUMO-E_HOMO. All polymers have high energy gaps, indicating stability that favors protecting the encapsulated molecule from unwanted interactions and premature degradation. Since polymers can adopt a variety of geometries, they are less likely to distort than $QPhNO_2$, which facilitates docking and interaction with the polymer chains used in nanoencapsulation. The simulations revealed that the PMMA/$QPhNO_2$, PCL/$QPhNO_2$, and PLGA/$QPhNO_2$ interactions had the lowest binding energies, at −4.60691, −4.43676, and −1.81392 kcal/mol, respectively. Moreover, a docking analysis shows that the polymers and the medication $QPhNO_2$ form non-bonded interactions. Additionally, simulations between the complex (polymer + $QPhNO_2$) and the surfactant Tween® 80 revealed extremely low binding energies, suggesting that its presence has no discernible impact on the drug release mechanism. In this context, all polymers were considered good candidates for encapsulation. These results will guide future experimental studies on the choice of polymer for nano-encapsulation of the $QPhNO_2$ molecule and provide insights into the kinetics of the drug delivery. The findings of this study will form the basis for future research on new analogs and molecular combinations. This work underscores the importance of computational chemistry in drug discovery and molecular characterization and demonstrates the effective use of these tools to improve drug nanoencapsulation. Additionally, it highlights the value of computational techniques in drug nanoencapsulation and stresses its importance in drug development.

Supplementary Materials: The following supporting information can be downloaded at: https://www.mdpi.com/article/10.3390/app15010468/s1, Details of the simulation settings performed in Spartan, including non-standard parameters and specific adjustments for theoretical calculations.

Author Contributions: Conceptualization, M.P.C., H.S.S., and E.N.d.S.J.; methodology, E.D.M., H.S.S., and R.G.A.; validation, E.D.M., I.F.S.R., and J.M.N.; formal analysis, E.D.M., I.F.S.R., and J.M.N.; investigation, E.D.M.; resources, E.C.d.S.-F., M.S.R., A.B.R., and H.S.S.; data curation, E.D.M., I.F.S.R., and J.M.N.; writing—original draft preparation, E.D.M., H.S.S., and M.P.C.; writing—review and editing, A.B.R., E.C.d.S.-F., and H.S.S.; visualization, A.B.R. and M.P.C.; supervision, M.P.C., H.S.S., and M.S.R.; project administration, M.P.C., H.S.S., and M.S.R. All authors have read and agreed to the published version of the manuscript.

Funding: This work was financially supported by the Coordination of the Improvement of Higher Education Personnel (CAPES) in the form of a scholarship (#8887.813947/2023-00).

Institutional Review Board Statement: Not applicable.

Informed Consent Statement: Not applicable.

Data Availability Statement: Data are contained within the article.

Acknowledgments: The authors thank UFPI and UFMG for structural support and the following Brazilian agencies: Coordination of the Improvement of Higher Education Personnel (CAPES) and the National Council for Scientific and Technological Development (CNPq). H.S.S. thanks Benildo Ferreira de Sousa, for the technical support regarding the computers used to carry out this work. E.N.S.J. would like to thank CNPq, CAPES, and FAPEMIG.

Conflicts of Interest: The authors declare no conflicts of interest.

References

1. Meyer, E.A.; Castellano, R.K.; Diederich, F. Interactions with Aromatic Rings in Chemical and Biological Recognition. *Angew. Chem.-Int. Ed.* **2003**, *42*, 1210–1250. [CrossRef] [PubMed]
2. Stefaniu, A.; Pintilie, L. Molecular Descriptors and Properties of Organic Molecules. In *Symmetry (Group Theory) and Mathematical Treatment in Chemistry*; InTech: Rijeka, Croatia, 2018; pp. 161–176.
3. Douroumis, D.; Fahr, A.; Siepmann, J.; Snowden, M.J.; Torchilin, V. *Computational Pharmaceutics: Application of Molecular Modeling in Drug Delivery*; John Wiley & Sons: Hoboken, NY, USA, 2015.
4. El Adam, S.; Bentley, C.; McQuarrie, L.; Teckle, P.; Peacock, S. Impact of a Cancer Diagnosis on the Income of Adult Cancer Survivors: A Scoping Review Protocol. *BMJ Open* **2021**, *11*, e047315. [CrossRef] [PubMed]
5. Mattiuzzi, C.; Lippi, G. Current Cancer Epidemiology. *J. Epidemiol. Glob. Health* **2019**, *9*, 217–222. [CrossRef] [PubMed]
6. Alam, S.; Khan, F. Virtual Screening, Docking, ADMET and System Pharmacology Studies on Garcinia Caged Xanthone Derivatives for Anticancer Activity. *Sci. Rep.* **2018**, *8*, 5524. [CrossRef]
7. da Silva Júnior, E.N.; de Souza, M.C.B.V.; Pinto, A.V.; Pinto, M.d.C.F.R.; Goulart, M.O.F.; Barros, F.W.A.; Pessoa, C.; Costa-Lotufo, L.V.; Montenegro, R.C.; de Moraes, M.O.; et al. Synthesis and Potent Antitumor Activity of New Arylamino Derivatives of Nor-β-Lapachone and nor-α-Lapachone. *Bioorg. Med. Chem.* **2007**, *15*, 7035–7041. [CrossRef]
8. Da Silva, E.N.; De Deus, C.F.; Cavalcanti, B.C.; Pessoa, C.; Costa-Lotufo, L.V.; Montenegro, R.C.; De Moraes, M.O.; Pinto, M.D.C.F.R.; De Simone, C.A.; Ferreira, V.F.; et al. 3-Arylamino and 3-Alkoxy-nor-β-Lapachone Derivatives: Synthesis and Cytotoxicity against Cancer Cell Lines. *J. Med. Chem.* **2010**, *53*, 504–508. [CrossRef]
9. Araújo, A.J.; de Souza, A.A.; da Silva Júnior, E.N.; Marinho-Filho, J.D.B.; de Moura, M.A.B.F.; Rocha, D.D.; Vasconcellos, M.C.; Costa, C.O.; Pessoa, C.; de Moraes, M.O.; et al. Growth Inhibitory Effects of 3′-Nitro-3-Phenylamino nor-Beta-Lapachone against HL-60: A Redox-Dependent Mechanism. *Toxicol. Vitr.* **2012**, *26*, 585–594. [CrossRef]
10. da Silva Júnior, E.N.; Jardim, G.A.M.; Jacob, C.; Dhawa, U.; Ackermann, L.; de Castro, S.L. Synthesis of Quinones with Highlighted Biological Applications: A Critical Update on the Strategies towards Bioactive Compounds with Emphasis on Lapachones. *Eur. J. Med. Chem.* **2019**, *179*, 863–915. [CrossRef]
11. Bolton, J.L.; Dunlap, T. Formation and Biological Targets of Quinones: Cytotoxic versus Cytoprotective Effects. *Chem. Res. Toxicol.* **2017**, *30*, 13–37. [CrossRef]
12. Kumagai, Y.; Shinkai, Y.; Miura, T.; Cho, A.K. The Chemical Biology of Naphthoquinones and Its Environmental Implications. *Annu. Rev. Pharmacol. Toxicol.* **2012**, *52*, 221–247. [CrossRef]
13. Costa, M.P.; Feitosa, A.; Oliveira, F.C.E.; Cavalcanti, B.C.; Da Silva, E.N.; Dias, G.G.; Sales, F.A.M.; Sousa, B.L.; Barroso-Neto, I.L.; Pessoa, C.; et al. Controlled Release of Nor-β-Lapachone by PLGA Microparticles: A Strategy for Improving Cytotoxicity against Prostate Cancer Cells. *Molecules* **2016**, *21*, 873. [CrossRef] [PubMed]
14. Fathi, M.; Martín, Á.; McClements, D.J. Nanoencapsulation of Food Ingredients Using Carbohydrate Based Delivery Systems. *Trends Food Sci. Technol.* **2014**, *39*, 18–39. [CrossRef]
15. Ahangaran, F.; Navarchian, A.H.; Picchioni, F. Material Encapsulation in Poly (Methyl Methacrylate) Shell: A Review. *J. Appl. Polym. Sci.* **2019**, *136*, 48039. [CrossRef]
16. Mittal, A.K.; Chisti, Y.; Banerjee, U.C. Synthesis of Metallic Nanoparticles Using Plant Extracts. *Biotechnol. Adv.* **2013**, *31*, 346–356. [CrossRef] [PubMed]
17. Bissessur, R.; Hopkins, B.; Dahn, D.C. Novel Nanocomposites: Intercalation of Ionically Conductive Polymers into Molybdic Acid. In *Encapsulation Nanotechnologies*; Wiley Online Library: Hoboken, NY, USA, 2013.

18. Fathi, M.; Mozafari, M.R.; Mohebbi, M. Nanoencapsulation of Food Ingredients Using Lipid Based Delivery Systems. *Trends Food Sci. Technol.* **2012**, *23*, 13–27. [CrossRef]
19. Ramanathan, S.; Lin, Y.C.; Thirumurugan, S.; Hu, C.C.; Duann, Y.F.; Chung, R.J. Poly(Methyl Methacrylate) in Orthopedics: Strategies, Challenges, and Prospects in Bone Tissue Engineering. *Polymers* **2024**, *16*, 367. [CrossRef]
20. Javaid, S.; Ahmad, N.M.; Mahmood, A.; Nasir, H.; Iqbal, M.; Ahmad, N.; Irshad, S. Cefotaxime Loaded Polycaprolactone Based Polymeric Nanoparticles with Antifouling Properties for In-Vitro Drug Release Applications. *Polymers* **2021**, *13*, 2180. [CrossRef]
21. Elmowafy, E.M.; Tiboni, M.; Soliman, M.E. Biocompatibility, Biodegradation and Biomedical Applications of Poly(Lactic Acid)/Poly(Lactic-Co-Glycolic Acid) Micro and Nanoparticles. *J. Pharm. Investig.* **2019**, *49*, 347–380. [CrossRef]
22. Sahu, A.; Solanki, P.; Mitra, S. Curcuminoid-Loaded Poly(Methyl Methacrylate) Nanoparticles for Cancer Therapy. *Int. J. Nanomed.* **2018**, *13*, 101–105. [CrossRef]
23. Guo, X.; Zuo, X.; Zhou, Z.; Gu, Y.; Zheng, H.; Wang, X.; Wang, G.; Xu, C.; Wang, F. PLGA-Based Micro/Nanoparticles: An Overview of Their Applications in Respiratory Diseases. *Int. J. Mol. Sci.* **2023**, *24*, 4333. [CrossRef]
24. Bhadran, A.; Shah, T.; Babanyinah, G.K.; Polara, H.; Taslimy, S.; Biewer, M.C.; Stefan, M.C. Recent Advances in Polycaprolactones for Anticancer Drug Delivery. *Pharmaceutics* **2023**, *15*, 1977. [CrossRef]
25. Khan, F.A.; Akhtar, S.; Almohazey, D.; Alomari, M.; Almofty, S.A.; Badr, I.; Elaissari, A. Targeted Delivery of Poly (Methyl Methacrylate) Particles in Colon Cancer Cells Selectively Attenuates Cancer Cell Proliferation. *Artif. Cells Nanomed. Biotechnol.* **2019**, *47*, 1533–1542. [CrossRef] [PubMed]
26. Elakkiya, K.; Bargavi, P.; Balakumar, S. 3D Interconnected Porous PMMA Scaffold Integrating with Advanced Nanostructured CaP-Based Biomaterials for Rapid Bone Repair and Regeneration. *J. Mech. Behav. Biomed. Mater.* **2023**, *147*, 106106. [CrossRef] [PubMed]
27. Taghiyar, H.; Yadollahi, B.; Kajani, A.A. Controlled Drug Delivery and Cell Adhesion for Bone Tissue Regeneration by Keplerate Polyoxometalate (Mo132)/Metronidazole/PMMA Scaffolds. *Sci. Rep.* **2022**, *12*, 14443. [CrossRef] [PubMed]
28. Zaszczyńska, A.; Kołbuk, D.; Gradys, A.; Sajkiewicz, P. Development of Poly(Methyl Methacrylate)/Nano-Hydroxyapatite (PMMA/NHA) Nanofibers for Tissue Engineering Regeneration Using an Electrospinning Technique. *Polymers* **2024**, *16*, 531. [CrossRef]
29. Shakya, A.K.; Al-Sulaibi, M.; Naik, R.R.; Nsairat, H.; Suboh, S.; Abulaila, A. Review on PLGA Polymer Based Nanoparticles with Antimicrobial Properties and Their Application in Various Medical Conditions or Infections. *Polymers* **2023**, *15*, 3597. [CrossRef]
30. Tilton, M.; Jacobs, E.; Overdorff, R.; Astudillo Potes, M.; Lu, L.; Manogharan, G. Biomechanical Behavior of PMMA 3D Printed Biomimetic Scaffolds: Effects of Physiologically Relevant Environment. *J. Mech. Behav. Biomed. Mater.* **2023**, *138*, 105612. [CrossRef]
31. Adeniji, S.E.; Uba, S.; Uzairu, A. Multi-Linear Regression Model, Molecular Binding Interactions and Ligand-Based Design of Some Prominent Compounds against Mycobacterium Tuberculosis. *Netw. Model. Anal. Health Inform. Bioinform.* **2020**, *9*, 8. [CrossRef]
32. Babatunde Olasupo, S. Density Functional Theory (B3LYP/6-31G*) Study of Toxicity of Polychlorinated Dibenzofurans. *Int. J. Comput. Theor. Chem.* **2017**, *5*, 14. [CrossRef]
33. Bouzzine, S.M.; Bouzakraoui, S.; Bouachrine, M.; Hamidi, M. Density Functional Theory (B3LYP/6-31G*) Study of Oligothiophenes in Their Aromatic and Polaronic States. *J. Mol. Struct. Theochem.* **2005**, *726*, 271–276. [CrossRef]
34. Oda, A.; Takahashi, O. Validation of ArgusLab Efficiencies for Binding Free Energy Calculations. *Chem-Bio Inform. J.* **2009**, *9*, 52–61. [CrossRef]
35. Tanguenyongwatana, P.; Jongkon, N. Molecular Docking Study of Tyrosinase Inhibitors Using ArgusLab 4.0.1: A Comparative Study. *Thai J. Pharm. Sci.* **2016**, *40*, 21–25. [CrossRef]
36. Hafeez, A.; Naz, A.; Naeem, S.; Bano, K.; Akhtar, N. Computational Study on the Geometry Optimization and Excited—State Properties of Riboflavin by ArgusLab 4.0.1. *Pak. J. Pharm. Sci.* **2013**, *26*, 487–493. [PubMed]
37. Meng, X.-Y.; Zhang, H.-X.; Mezei, M.; Cui, M. Molecular Docking: A Powerful Approach for Structure-Based Drug Discovery. *Curr. Comput. Aided-Drug Des.* **2012**, *7*, 146–157. [CrossRef]
38. Demir, P.; Akman, F. Molecular Structure, Spectroscopic Characterization, HOMO and LUMO Analysis of PU and PCL Grafted onto PEMA-Co-PHEMA with DFT Quantum Chemical Calculations. *J. Mol. Struct.* **2017**, *1134*, 404–415. [CrossRef]
39. Santos, L.H.S.; Ferreira, R.S.; Caffarena, E.R. Integrating Molecular Docking and Molecular Dynamics Simulations. In *Docking Screens for Drug Discovery*; Springer: Berlin/Heidelberg, Germany, 2019; pp. 13–34.
40. Viswanadhan, V.N.; Ghose, A.K.; Revankar, G.R.; Robins, R.K. Atomic Physicochemical Parameters for Three Dimensional Structure Directed Quantitative Structure-Activity Relationships. 4. Additional Parameters for Hydrophobic and Dispersive Interactions and Their Application for an Automated Superposition of Certain Naturally Occurring Nucleoside Antibiotics. *J. Chem. Inf. Comput. Sci.* **1989**, *29*, 163–172. [CrossRef]
41. Senapati, S.; Mahanta, A.K.; Kumar, S.; Maiti, P. Controlled Drug Delivery Vehicles for Cancer Treatment and Their Performance. *Signal Transduct. Target. Ther.* **2018**, *3*, 7. [CrossRef]

42. Shao, Y.; Molnar, L.F.; Jung, Y.; Kussmann, J.; Ochsenfeld, C.; Brown, S.T.; Gilbert, A.T.B.; Slipchenko, L.V.; Levchenko, S.V.; O'Neill, D.P.; et al. Advances in Methods and Algorithms in a Modern Quantum Chemistry Program Package. *Phys. Chem. Chem. Phys.* **2006**, *8*, 3172–3191. [CrossRef]
43. Hughes, J.D.; Blagg, J.; Price, D.A.; Bailey, S.; DeCrescenzo, G.A.; Devraj, R.V.; Ellsworth, E.; Fobian, Y.M.; Gibbs, M.E.; Gilles, R.W.; et al. Physiochemical Drug Properties Associated with in Vivo Toxicological Outcomes. *Bioorg. Med. Chem. Lett.* **2008**, *18*, 4872–4875. [CrossRef]
44. Shi, J.; Kantoff, P.W.; Wooster, R.; Farokhzad, O.C. Cancer Nanomedicine: Progress, Challenges and Opportunities. *Nat. Rev. Cancer* **2017**, *17*, 20–37. [CrossRef]
45. Alsaigh, R.A.; Rahman, S.; Alfaifi, F.S.; Al-Gawati, M.A.; Shallaa, R.; Alzaid, F.; Alanazi, A.F.; Albrithen, H.; Alzahrani, K.E.; Assaifan, A.K.; et al. Detection of Volatile Alcohol Vapors Using PMMA-Coated Micromechanical Sensors: Experimental and Quantum Chemical DFT Analysis. *Chemosensors* **2022**, *10*, 452. [CrossRef]
46. Hazim, A.; Abduljalil, H.M.; Hashim, A. Design of PMMA Doped with Inorganic Materials as Promising Structures for Optoelectronics Applications. *Trans. Electr. Electron. Mater.* **2021**, *22*, 851–868. [CrossRef]
47. Soltani, A.; Khan, A.; Mirzaei, H.; Onaq, M.; Javan, M.; Tavassoli, S.; Mahmoodi, N.O.; Arian Nia, A.; Yahyazadeh, A.; Salehi, A.; et al. Improvement of Anti-Inflammatory and Anticancer Activities of Poly(Lactic-Co-Glycolic Acid)-Sulfasalazine Microparticle via Density Functional Theory, Molecular Docking and ADMET Analysis. *Arab. J. Chem.* **2022**, *15*, 103464. [CrossRef]
48. Kumari, A.; Yadav, S.K.; Yadav, S.C. Biodegradable Polymeric Nanoparticles Based Drug Delivery Systems. *Colloids Surf. B Biointerfaces* **2010**, *75*, 1–8. [CrossRef]
49. Parambil SH, K.; Parambil HA, T.; Hamza, S.P.; Parameswaran, A.T.; Thayyil, M.S.; Karuvanthodi, M. DFT and Molecular Docking Studies of a Set of Non-Steroidal Anti-Inflammatory Drugs: Propionic Acid Derivatives. In *Density Functional Theory Calculations*; IntechOpen: London, UK, 2021.
50. Leal, A.L.A.B.; Pinheiro, D.P.; Barros-Nepomuceno, F.W.A.; da Silva, P.T.; Pessoa, C.; Almeida-Neto, F.W.Q.; Marinho, E.S.; Barreto, A.C.H.; Julião, M.S.S.; de Paiva, A.S.; et al. Structural and Spectroscopic Analysis and Evaluation of Cytotoxic Activity of 2-Hydroxychalcones against Human Cancer Cell Lines. *J. Mol. Struct.* **2021**, *1245*, 131135. [CrossRef]
51. Politzer, P.; Murray, J.S.; Concha, M.C. The Complementary Roles of Molecular Surface Electrostatic Potentials and Average Local Ionization Energies with Respect to Electrophilic Processes. *Int. J. Quantum Chem.* **2002**, *88*, 19–27. [CrossRef]
52. Dong, E.; Huo, Q.; Zhang, J.; Han, H.; Cai, T.; Liu, D. Advancements in Nanoscale Delivery Systems: Optimizing Intermolecular Interactions for Superior Drug Encapsulation and Precision Release. *Drug Deliv. Transl. Res.* **2025**, *15*, 7–25. [CrossRef]
53. Sanchez-Sanchez, A.; Pomposo, J.A. Single-Chain Polymer Nanoparticles via Non-Covalent and Dynamic Covalent Bonds. *Part. Part. Syst. Charact.* **2014**, *31*, 11–23. [CrossRef]
54. Cronin, D.; Mark, T. The Role of Hydrophobicity in Toxicity Prediction. *Curr. Comput. Aided-Drug Des.* **2006**, *2*, 405–413. [CrossRef]
55. Cronin, M.T. *Predicting Chemical Toxicity and Fate*; CRC press: London, UK, 2004.
56. Abraham, M.H.; Duce, P.P.; Prior, D.V.; Barratt, D.G.; Morris, J.J.; Taylor, P.J. Hydrogen Bonding. Part 9. Solute Proton Donor and Proton Acceptor Scales for Use in Drug Design. *J. Chem. Soc. Perkin Trans. 2* **1989**, 1355–1375. [CrossRef]
57. Iakovou, G.; Laycock, S.D.; Hayward, S. Interactive Flexible-Receptor Molecular Docking in Virtual Reality Using DockIT. *J. Chem. Inf. Model.* **2022**, *62*, 5855–5861. [CrossRef] [PubMed]
58. Chaudhary, M.; Tyagi, K. A REVIEW ON MOLECULAR DOCKING AND IT'S APPLICATION. *Int. J. Adv. Res.* **2024**, *12*, 1141–1153. [CrossRef]
59. Albano, J.M.R.; de Paula, E.; Pickholz, M. Molecular Dynamics Simulations to Study Drug Delivery Systems. In *Molecular Dynamics*; IntechOpen: London, UK, 2018.
60. Aulifa, D.L.; Al Shofwan, A.A.; Megantara, S.; Fakih, T.M.; Budiman, A. Elucidation of Molecular Interactions Between Drug–Polymer in Amorphous Solid Dispersion by a Computational Approach Using Molecular Dynamics Simulations. *Adv. Appl. Bioinform. Chem.* **2024**, *17*, 1–19. [CrossRef]
61. Salo-Ahen, O.M.H.; Alanko, I.; Bhadane, R.; Alexandre, A.M.; Honorato, R.V.; Hossain, S.; Juffer, A.H.; Kabedev, A.; Lahtela-Kakkonen, M.; Larsen, A.S.; et al. Molecular Dynamics Simulations in Drug Discovery and Pharmaceutical Development. *Processes* **2021**, *9*, 71. [CrossRef]